Journal of Thermal Science Vol.31, No.6 (2022) 2189–2202

**https://doi.org/10.1007/s11630-022-1686-6** **Article ID: 1003-2169(2022)06-2189-14**

# Morphology Structure Evolution and Combustion Reactivity of Bituminous Char at Around Ash Melting Temperature

**ZHANG Yandi, YANG Huan, WANG Bo, H.M. Shahzaib KHAN, DUAN Xiaoli, LIU Yinhe***

State Key Laboratory of Multiphase Flow in Power Engineering, Xi'an Jiaotong University, Xi'an 710049, China

© Science Press, Institute of Engineering Thermophysics, CAS and Springer-Verlag GmbH Germany, part of Springer Nature 2022

**Abstract:** In slag tapping furnaces, char particles undergo a series of complex structural evolution before and after being captured by the liquid slag layer. The evolution results affect the carbon conversion rate and are affected by temperature fluctuations, especially in the ash melting temperature zone. Experimental study on structure evolution of bituminous char prepared at around ash melting temperature was carried out on a fixed bed. The morphology, specific surface area and mineral chemical composition were measured at different temperatures. Experimental results show that the number density and the size of ash droplets exuded on the char surface increased significantly with the increasing temperature. The ash specific surface area from gasification was slightly greater than that from combustion. The residual content of chloride in the char become 1% and the contents of Fe, K, Mg and Na decrease significantly during the pyrolysis process across the ash melting temperature zone. The diffraction intensity of oldhamite increase which indicates the reaction of carbon substrate with minerals during the evolution; the diffraction intensity of quartz dramatically decreases for the reason of anorthite generation. The ignition and burnout temperatures of char were found to increase and the combustion stability decreased with the increasing pyrolysis temperature.

**Keywords: coal char, structure evolution, carbothermal reaction, combustion**

## 1. Introduction

Coal is the dominant energy source in China and some other developing countries. In the process of coal utilization such as combustion and gasification, the minerals may cause a series of ash related issues including deposition, fouling, corrosion or erosion in furnace [1–4]. During these thermal treating processes, ash stickiness plays a crucial role in determining whether the ash particle will stick to the heat transfer surface or rebound [5]. Therefore, ash stickiness has been studied extensively in terms of ash chemistry, temperature, viscosity, and the fraction of molten phase. Conventional ash fusion temperature (AFT) tests are usually used to predict the fusibility of ash. The ash fusion temperature depends upon the composition of ash in coal. Furthermore, the formed fly ashes smaller than micron scale may also contribute to the fine particulate emission [6, 7]. Increasing the capture efficiency of particles on the dry or wet surface and reducing the formation of fine ash particulates are two methods of minimizing fine ash emission [8].

The above-mentioned issues could all come down to ash related problems [9], which are all associated with the char structure evolution during the gasification and combustion process. It is of great significance to clarify the coal-char-slag transition mechanism at high temperature range. In slagging gasifier and boiler,

Received: Jun 9, 2020 AE: YANG Bin Corresponding author: LIU Yinhe E-mail: yinheliu@mail.xjtu.edu.cn

char-slag transformation may influence char structure and particle deposition behavior on the slagging surface. For highly converted char, the ash exposed on the particle surface may be captured by the slagging layer on the furnace wall due to the stickiness between the ashes on the char particle and the molten slag [10]. The char particles with lower conversion ratio have weaker adhesion force between char and molten slag [11], so the probability of rebounding to the gas phase is bigger than that of higher conversion ratio after they dash on the slagging wall. In addition, among the char particles captured by the slag layer, the char particles with higher activity are gasified or burned [12], while the lower activity char particles remained incompletely transformed, and gradually covered by the slag to form residual carbon. When the residual carbon content in the slag is high, the phenomenon of slag blocking may occur, which seriously affects the safe operation of the equipment. Therefore, the char-slag transition and the char structure are very important for the slagging layer maintenance and the flow of molten slag [13]. According to the actual situation, the variable load often affects the working temperature, while the operating temperature is the main factor affecting the conversion of coal char. The structural evolution process of the coal char before being captured by the slag layer and the process of combustion or gasification or storage after capture are affected by temperature fluctuations, especially in the ash melting temperature zone.

Many researchers investigated the micromorphology, specific surface area, pore structure, carbon crystallite structure, mineral transformation and gasification reactivity of the char prepared at different atmospheres on one dimension reactor [14–19]. However, the behavior of the coal structure evolution such as the variation of the specific surface area and the mineral transformation at different temperature range has not been clearly clarified, especially in the ash melting temperature zone. Besides, most of those previous studies did not pay much attention to the influence of ash fusion on the evolution of char structure which is of vital importance to the combustion and gasification, and the relationship between the coal char structure evolution and char combustion reactivity in the ash melting temperature zone still needs further study.

The evolution of the char, which is composed of fixed carbon and ash, includes the fixed carbon evolution, ash evolution and the interaction between fixed carbon and ash at high temperature. When coal char particles are heated from ambient temperature to that higher than ash melting point, polycondensation of fixed carbon in char takes place. Dehydrogenation condensation of aromatic structures and the increase of aromatic layers take place [20, 21]. At the same time of the fixed carbon polycondensation, the mineral matters in char also undergo a series of decomposition or combination reactions at high temperature [22–26]. Ma et al. [27] used the muffle and radio frequency oxygen plasma furnace to prepare the high and low temperature coal ash, respectively. The results showed that the minerals play an important role in the gasification and combustion process.

The melting behavior of ash during char reaction may influence the reactivity of the char. Wu et al. [25] studied mineral reactions and morphology of ash during char gasification in $CO_2/H_2O$ atmosphere at high temperature. They concluded that some molten or semi-molten parts of ash may adhere to the coal char surface and blocked some micropores in char. Radovic et al. [28] found that molten ash blocked the internal pores of the char, decreased the reaction surface area and thus reduced the char reactivity. Ding et al. [29] also agreed with the statements that ash fusion behavior is of vital importance to the gasification process of char, and they found that there was a threshold value ($x$=0.9) of gasification conversion for Yunnan lignite and Shenfu bituminous above the ash fusion temperature.

Ash sintering and melting processes may influence the specific surface area (SSA) and pore structure of the char particles, further to change the reactivity of char. Li et al. [30] found that the SSA and total pore volume increased as the pyrolysis temperature rised from 900°C to 1100°C. Wang et al. [31] found the SSA of char for two bituminous coals decreased obviously when pyrolysis increased from 1100°C to 1500°C, which was consistent with the conclusion that Zhang et al. [32] got. Wei et al. [33] thought that biomass ash additives had positive effect on the pore structure and carbon structure of coal char. Consistency has not been reached about the effect of final pyrolysis temperature on the specific surface area of coal char prepared at high temperature over 1000°C. Mechanism about volatile release on the SSA increase, fixed carbon polycondensation and ash clinkering on the SSA decrease are still unclear.

The interaction between ash and fixed carbon determines the char-slag transition process. Raask et al. [34] and Lin et al. [35] found that coal-ash slag drops contracted forming spheres and they did not soak into char matrix. Miccio et al. [36] simulated the flow and agglomeration behavior of molten ash particles using Monte Carlo method; they concluded that the melted ash might form small droplets on the char surface and then agglomerate to form bigger ash spheres if the fragmentation of the char does not occur. Whereas Latorre et al. [37] considered that only part of the minerals in char aggregated, and the other part formed fly ash separately. In addition, the fixed carbon also influences the chemical composition of the ash due to the existence of carbothermic reaction. CaO, $Fe_3O_4$, $SiO_2$, kaolinite etc. were all confirmed to react with the carbon

matrix to generate new minerals [38–40].

The coal particles fed into the furnace undergo drying and devolatilization to form char particles. Pyrolysis, gasification and combustion of the char may occur according to the reaction condition. A series of changes in terms of the micromorphology, SSA, pore structure, element and mineral composition might take place in those processes with the evolution processes such as ash sintering, ash fusion, fixed carbon polycondensation and consumption [41–44]. In present paper, Lu'an bituminous coal was used to prepare the char/ash in Ar, $CO_2$ and air atmosphere at ash fusion temperature range. The scanning electron microscope-energy dispersive X-ray spectrometer (SEM-EDS), specific surface analysis (SSA), X-ray fluorescence analysis (XRF), X-ray diffraction analysis (XRD), FactSage7.3 and thermogravimetric analyzer (TGA) were performed in order to clarify the mechanism of ash percolation, ash coalescence, ash-char interaction, char structure evolution and char combustion reactivity during the thermal treatment.

## 2. Experiment and Methods

### 2.1 Experimental apparatus

Figure 1 shows the experimental system of fixed bed for the preparation of char and ash. The corundum reaction tube is 40 mm for inner diameter and length is 1200 mm, and the heating section of the reaction tube is 800 mm. The tube is heated by electric heating furnace which is controlled by a temperature controller with the uncertainty of 3°C. An S-type thermal couple was used to measure the temperature of the fixed bed experimental system.

### 2.2 Coal sample

Lu'an bituminous coal from Shanxi Province in China was selected for present study due to the huge reserves and high representation. Parent coal samples were air-dried, grinded, and sieved to size of 91–125 μm. Table 1 shows the ultimate and proximate analysis (5E-MAG6600 analyzer, China) of Lu'an bituminous coal. Table 2 gives the results of ash composition which performed by the semi micro chemical analysis method and atomic absorption method according to Chinese standard GB/T1547-2007. The ash fusion characteristics were determined by HR-8 ash fusion point meter produced in China. The deformation temperature (DT), softening temperature (ST), hemisphere temperature (HT) and fluid temperature (FT) are 1140°C, 1180°C, 1190°C and 1200°C, respectively.

### 2.3 Experimental conditions and procedure

In our previous work [45], it was found that when char making in the nitrogen atmosphere, minerals would react

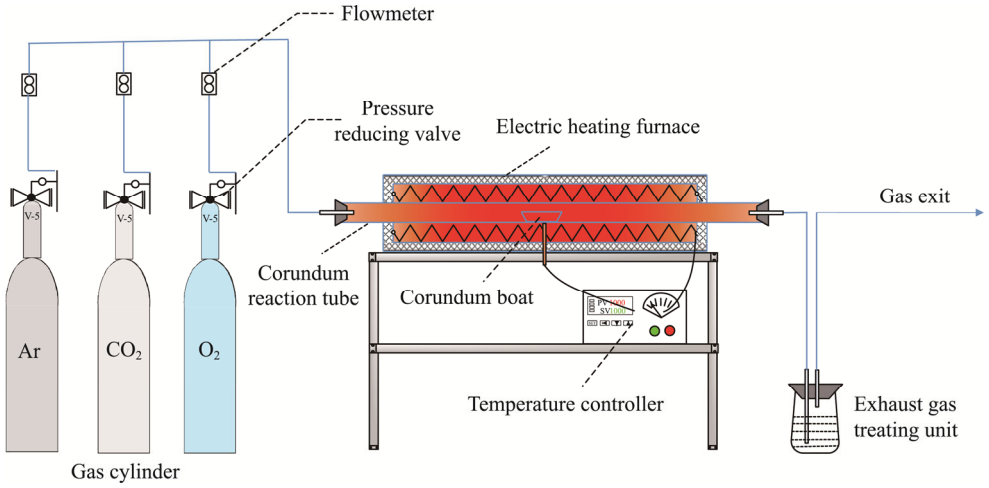


**Fig. 1** Experimental system of fixed bed for bituminous char/ash preparation

**Table 1** Ultimate and proximate analysis of Lu'an bituminous coal (air-dried basis)

| Proximate analysis/wt% | | | | Ultimate analysis/wt% | | | | |
|---|---|---|---|---|---|---|---|---|
| $M_{ad}$ | $A_{ad}$ | $V_{ad}$ | $FC_{ad}$ | $C_{ad}$ | $H_{ad}$ | $N_{ad}$ | $S_{ad}$ | $O_{ad}$* |
| 6.83 | 10.92 | 31.78 | 50.47 | 61.35 | 2.97 | 0.57 | 0.14 | 17.22 |

M: moisture; A: ash; V: volatile; FC; fixed carbon; ad: air dried. * Calculated by difference.

**Table 2** Ash composition analysis of Lu'an bituminous coal (unit: wt%)

| $SiO_2$ | $Al_2O_3$ | $Fe_2O_3$ | CaO | MgO | $Na_2O$ | $K_2O$ | $TiO_2$ | $SO_3$ |
|---|---|---|---|---|---|---|---|---|
| 36.75 | 16.32 | 6.46 | 27.54 | 2.74 | 2.90 | 0.24 | 0.94 | 3.70 |

with nitrogen to form flocculent substances on the surface of particles, which would have a certain impact on the structure of coal char. Therefore, the argon (Ar) atmosphere was used for char making in this work. Lu'an bituminous coal was placed under Ar atmosphere for 60 min to undergo a pyrolysis process in the fixed bed to prepare char sample for subsequent analysis. With the purpose to obtain the evolution of ash structure with heating temperature, Lu'an coal was heated in pure $CO_2$ for 60 mins and air atmosphere for 60 min, respectively. Three mass flow controllers were used to adjust the flow rate of Ar, $CO_2$ and $O_2$ of high purity to simulate the atmosphere of pyrolysis with pure Ar, gasification with pure $CO_2$ and combustion with 21 vol% $O_2$ and 79 vol% Ar.

Detailed procedures are as follows: Firstly, the empty furnace was preheated to a certain temperature according to the reaction's request, and then the specified gas was beforehand injected to fill the reaction tube. Reaction gas entered the reaction tube from the left and then went out from the right of the tube with the total flow rate of 1 L/min. About 1.5 g parent Lu'an coal was paved uniformly in the corundum boat with the thickness of 1 mm. The corundum boat was put into the preparing section, and then rapidly pushed into the heating section which was preheated to the reaction temperature, and finally to the cooling section. The heating temperature is in the range of 900°C to 1300°C at the interval of 100°C, according to the fusibility of parent coal ash.

### 2.4 Analysis methods

#### 2.4.1 Scanning electron microscope-energy dispersive X-ray spectrometer analysis

SEM combined with an energy-dispersive X-ray analyzer is one of the best methods to determine the microstructural and corresponding chemical composition features of ash during coal conversion under both combustion and gasification conditions [46, 47]. A field emission scanning electron microscope (SEM JSM-6390A, Japan) equipped with an energy dispersive X-ray spectrometer manufactured by JEOL Ltd was used to observe the surface morphology change of char/ash samples. The image was captured at backscattered electron (BSE) mode. EDS was used for the qualitative element identification and distribution with an information depth of approximately 3–5 μm from the particle surface [48]. The SEM-EDS analysis was performed on particle samples by operating SEM at an accelerating voltage of 15 kV, beam spot size of 40 nm and working distance of 10 mm in *Z* direction.

#### 2.4.2 Specific surface analysis

Rise-1010 automatic specific surface area analyzer was used to measure the SSA of coal/char/ash by the low temperature nitrogen physical adsorption method. Rise-1010 has high precision for the porous sample whose SSA is larger than 0.001 $m^2/g$. In present study, SSA of all the samples is higher than 3 $m^2/g$. The uncertainty of absolute pressure gauge is within 0.12%, and the temperature is 0.1°C.

#### 2.4.3 X-ray fluorescence analysis

X-ray fluorescence, often occupied in the field of coal chemical industry, was used to measure the element content in raw coal and char prepared under different pyrolysis temperatures. Manufactured in Bruker of Germany, the instrument (S4PIONEER) could provide a relative accurate element content from Be4 to U92, with content range from sub-ppm to 100%. The results were typically given as the percentage of elemental oxide.

#### 2.4.4 X-ray diffraction analysis

X-ray diffractomer was used to give the mineral information of coal char prepared at different temperatures. X-ray diffraction patterns were recorded on Bruker D8 Advance X-ray diffractomer operating at 40 kV and 40 mA with Cu Kα radiation over 10°–90°. The wave length of the instrument is $1.54\times10^{-10}$; the scanning speed and step size are 4°/min and 0.02°, respectively. The patterns of diffraction were analyzed with the help of Jade 6.

#### 2.4.5 Thermodynamic calculation

The thermodynamic software package FactSage7.3 was used to calculate the Gibbs free energy change ($\Delta G$) of different reactions to clearly study the mechanism of the mineral transformation in char during the thermal treatment process. The calculation is based on minimization of Gibbs free energy [49]. The isothermal reaction properties of a stoichiometric reaction between the minerals are determined by the Reaction module in FactSage. The FactPS, FToxid and FTsalt databases were chosed for calculation. $\Delta G$ was chosen to evaluate the possibility of mineral reactions in this work, which has also been used by other researchers [50].

#### 2.4.6 Thermogravimetric analyzer

Labsys Evo simultaneous thermal analyzer manufactured by Cetaram Company of France was used for thermogravimetric analysis, and the kinetic parameters of the reaction were calculated based on the results of thermal mass loss curve and thermal mass loss rate curve (TG-DTG). The specific experimental conditions are as follows: The char samples were weighed to (10±0.1) mg and placed in an alumina crucible. The kinetic parameters of combustion reaction were determined by 60 mL/min components of 85 vol% $N_2$ and 15 vol% $O_2$. The reaction temperature range is 30°C–1200°C and the heating rate is controlled to 20°C/min.

## 3. Results and Discussion

### 3.1 Effect of temperature on micro-morphology of char/ash under different atmosphere

#### 3.1.1 Evolution of micro-morphology of char under pyrolysis atmosphere

Lu'an bituminous coal was pyrolyzed under Ar atmosphere in the fixed bed as shown in Fig. 1. The produced char was scanned under JSM-6390A SEM to find the overall structure and micro-morphology change with the pyrolysis temperature. Fig. 2 gives the morphology of Lu'an bituminous chars pyrolyzed under inert Ar for 60 min at different temperatures.

There are some highlighted areas identified by the boxes scattered on the surface of each char to some extent in Fig. 2. Taking the 1300°C char as an example, the EDS analysis was performed to investigate the

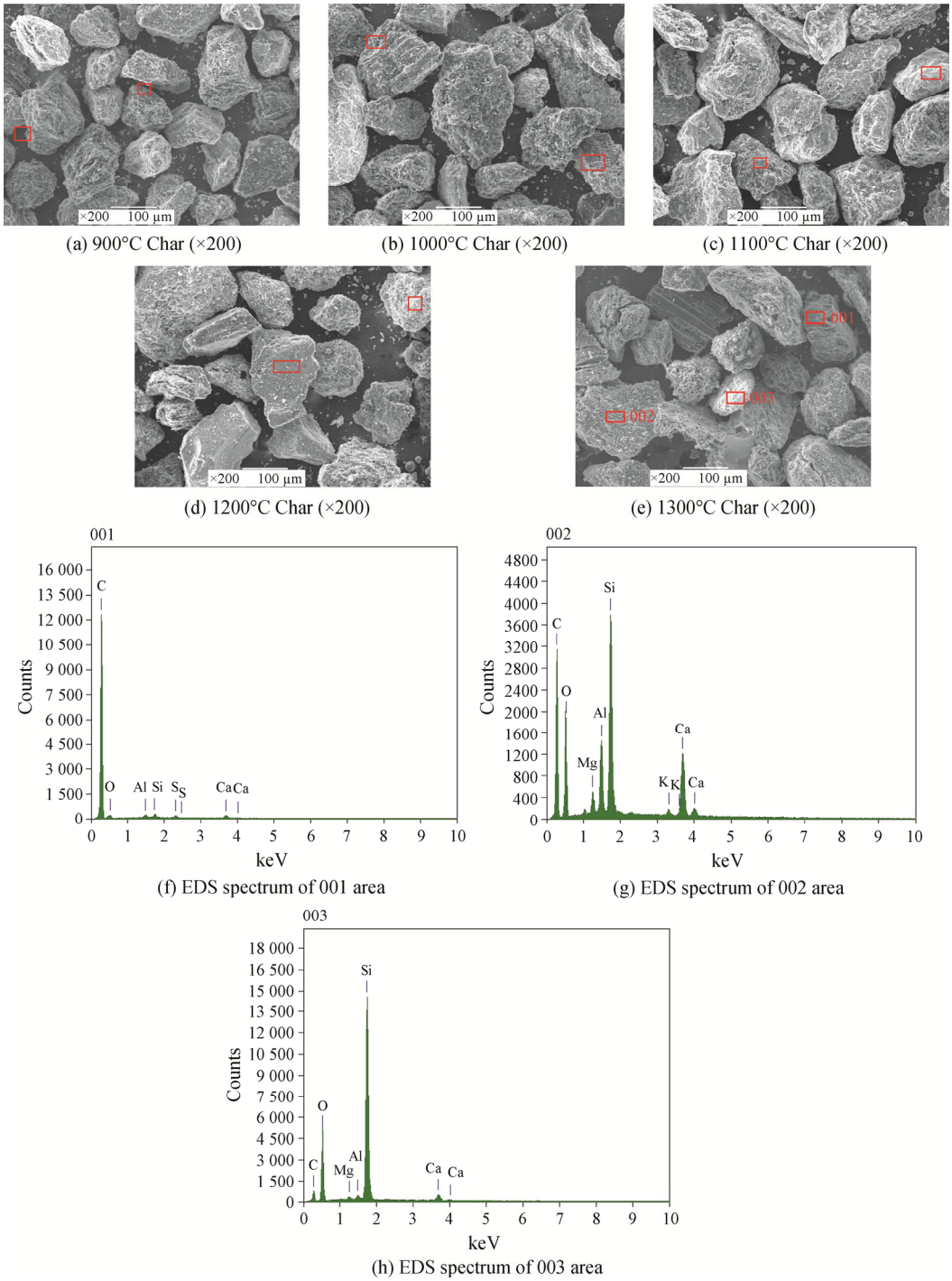


(a) 900°C Char (×200) (b) 1000°C Char (×200) (c) 1100°C Char (×200)

(d) 1200°C Char (×200) (e) 1300°C Char (×200)

(f) EDS spectrum of 001 area (g) EDS spectrum of 002 area

(h) EDS spectrum of 003 area

**Fig. 2** SEM analysis of bituminous char prepared at different temperatures under Ar

difference between highlighted area and non-highlighted area under the SEM. It is clearly demonstrated that the elements in non-highlighted areas are mainly carbon, whereas high concentration of mineral elements such as Si, Al, Ca and Mg are observed in highlighted area. Obviously, those enriched elements mainly exist in the minerals of char for the fact that the brightness of the secondary electron image for mineral is higher than that for organic maceral [51]. Therefore, the highlighted areas in Fig. 2 are caused by high concentration of minerals. It is worth noting that the uniformity of the distribution of ash spheres on the char surface may have an impact on the ash melting behavior [48].

The minerals in parent coal may decompose and react to form ash (different from minerals in parent coal) during the pyrolysis at temperature across the ash melting temperature range. In order to investigate the exudation, coalescence and detachment of ash during the char evolution process, the char at different temperatures were observed in SEM with high magnitude. The micro-morphology of char is depicted in Fig. 3.

As can be seen from Fig. 3, more ash spheres exude on the char particle surface at higher pyrolysis temperature. Molten ash on the surface of the char particle will aggregate to form spheres because of the surface tension. In the range of 900°C–1200°C; the number density of small ash spheres increases with the pyrolysis temperature, and the average size of ash spheres also enlarges. When the temperature rises to 1300°C, ash spheres enlarge dramatically under the SEM. The viscosity of molten ash decreases and the fluidity increases with the increase of pyrolysis temperature. As a result, the adjacent molten ash spheres grow up, aggregate, and merge to be a larger ash block above the ash fusion temperature. When two liquid ash spheres contact each other, the liquid surface will shrink because of the surface tension and thus a concave neck is formed between the ends of the liquid phase at the junction of ash particles as shown in Fig. 3(e).

In order to observe the char morphology more clearly at different pyrolysis temperatures, the area in Fig. 3(e) was magnified under 5000 times on SEM and the result was shown in Fig. 3(f). Fig. 3(f) presents that part of the molten ash percolated from coal char occupies part of the channel in the char particle as shown in box 1 and box 2, which may cause the blockage of macro pores structure. Part of the molten ash aggregates at the outlet of pores: on the one hand, the melted ash blocks the whole cross section as indicated in box 3 which makes the open pore completely closed; on the other hand, the molten ash percolates at the exit of pore causing partial blockage of the macro pores as box 4 shown, Bai et al. [18] also observed this phenomenon in their study.

### 3.1.2 Evolution of micro-morphology of ash during gasification/combustion

In order to explore the evolution behavior of ash structure in the process of char gas phase transformation across ash melting temperature, gasification ash and combustion ash at different temperatures were prepared respectively. Fig. 4 shows the microstructure of gasification ash prepared at 900°C–1100°C under $CO_2$ atmosphere. Fig. 5 shows the microstructure of combustion ash prepared under 21 vol% $O_2$ and 79 vol% Ar atmosphere. The SEM analysis for temperature above 1200°C was not performed because the ash was melted and stuck to the corundum boat after gasification/ combustion.

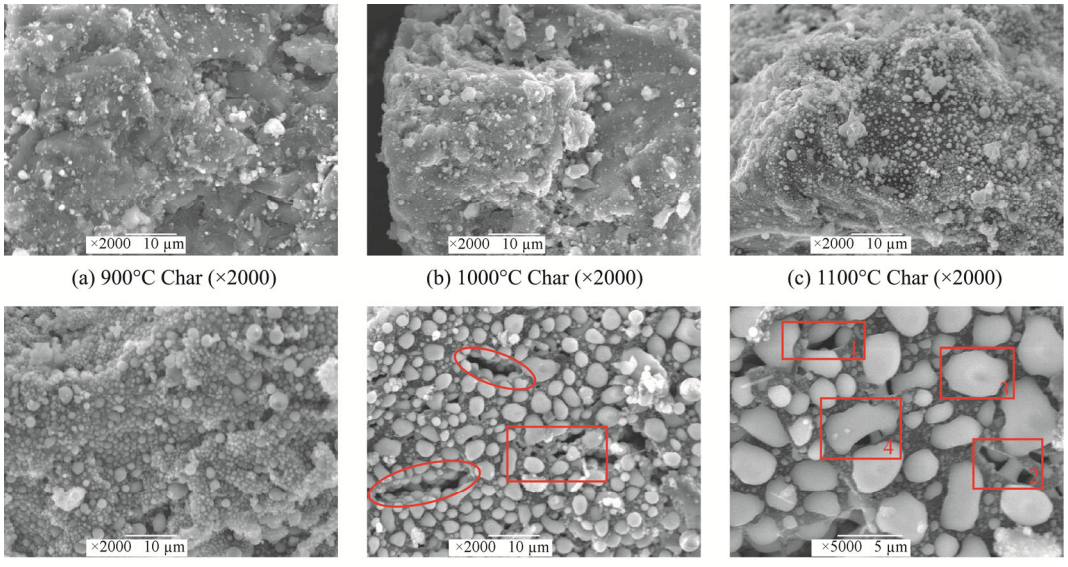


(a) 900°C Char (×2000) (b) 1000°C Char (×2000) (c) 1100°C Char (×2000)

(d) 1200°C Char (×2000) (e) 1300°C Char (×2000) (f) 1300°C Char (×5000)

**Fig. 3** Micromorphology of char prepared under Ar at different temperatures

Fig. 4 shows that both ash particles of about 100 um and small particle fragments of various sizes exist. Ash fragments increase with the reaction temperature, which demonstrates that all the minerals in char are not fully connected to form an ash skeleton. There are many open and tiny pores in the ash particles at 900°C; as the gasification temperature increases, pores of ash particles enlarge. When the temperature rises to 1100°C, it can be seen from SEM images under 2000 times that deformation of surface morphology occurs, and the sharp edge of the particle becomes round although the temperature does not reach the melting temperature. Lin et al. [35] also observed that the Newlands ash began melting at about 190°C below ST, which is consistent with the result of the present study.

Fig. 5 presents that the ash has well developed pore structure for combustion at 900°C. As the combustion temperature rises to 1000°C, there is a trace of deformation; the sharp end and convex part become round and the number density of pore decreases. When combustion temperature reaches 1100°C, there are abundant round ash droplets, which suggest that high temperature promotes the deformation of ash particles and the appearance of ash softening phenomenon. Wang et al. [52] also observed this phenomenon during the biomass briquettes combustion.

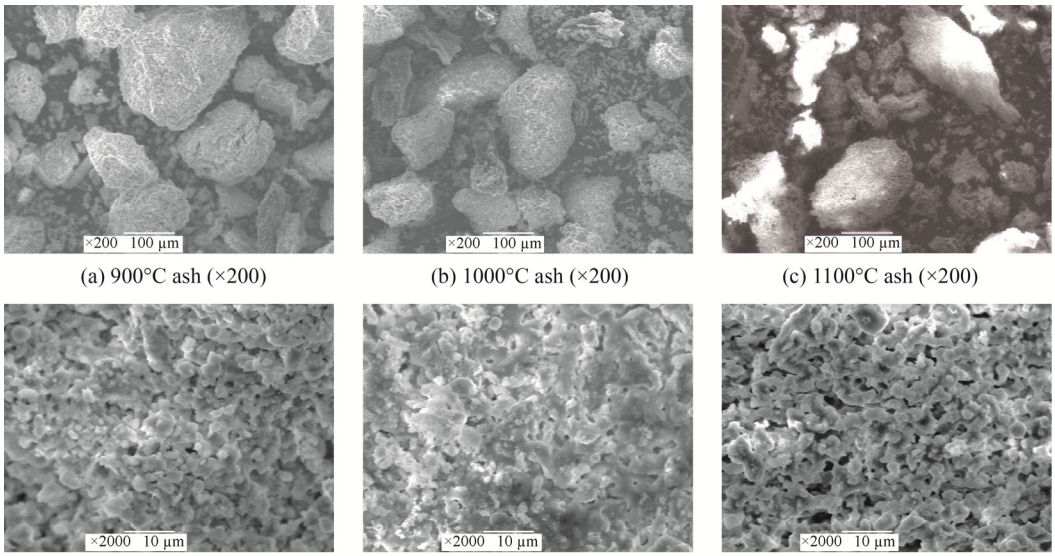


(a) 900°C ash (×200) (b) 1000°C ash (×200) (c) 1100°C ash (×200)

(d) 900°C ash (×2000) (e) 1000°C ash (×2000) (f) 1100°C ash (×2000)

**Fig. 4** SEM analysis of bituminous ash prepared at different gasification temperatures

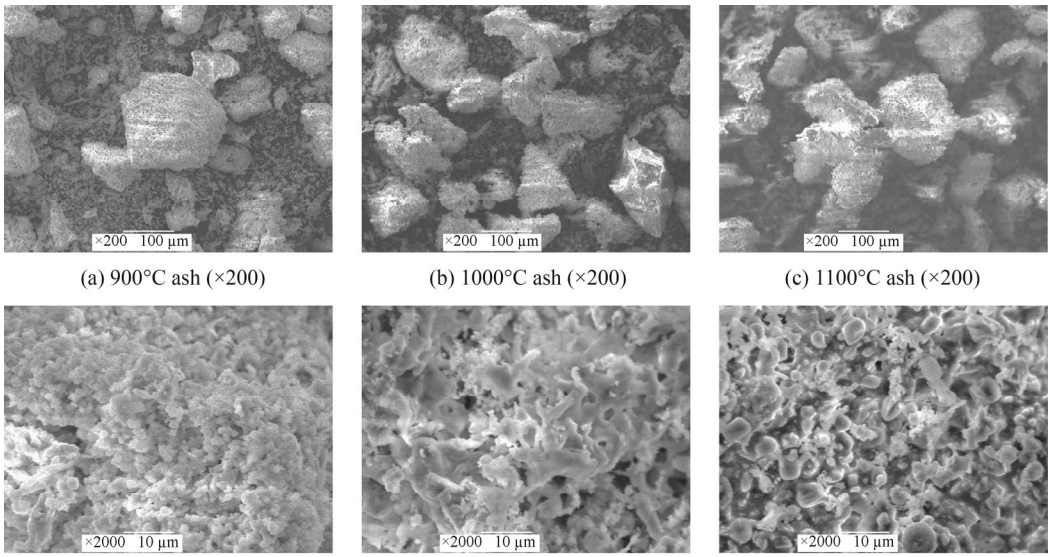


(a) 900°C ash (×200) (b) 1000°C ash (×200) (c) 1100°C ash (×200)

(d) 900°C ash (×2000) (e) 1000°C ash (×200) (f) 1100°C ash (×2000)

**Fig. 5** SEM analysis of bituminous ash prepared at different combustion temperatures

### 3.2 Effect of temperature on specific surface area of char/ash

The SSA of char/ash was measured and the results are shown in Fig. 6. From Fig. 6, the SSA of char prepared in Ar pyrolysis is the largest, followed by that of ash prepared in $CO_2$ gasification, and the SSA of ash prepared in the air is the smallest at the same temperature. Ashing in $CO_2$ and air atmosphere are the same in terms of mechanism, which is the destruction and consumption of carbon structure. The transport effects, concentrations and temperature will all affect the specific surface area of the coal ash [53]. While, the main influencing factor is the difference of particle surface temperature caused by reaction endothermic effect or exothermic effect. Particle temperature for gasification is lower than that of combustion [54], resulting in relatively low damage to the structure of ash particles, which leads to the greater SSA for gasification than that for combustion at the same reaction temperature.

As described above, in the range across the ash melting temperature, the SSA decrease of the coal char with the rising pyrolysis temperature might be attributed to the following factors: char polycondensation, ash sintering and ash fusion. According to the dominating mechanism for SSA reduction at different reaction temperatures, the pyrolysis process of the coal char across ash melting temperature range could be divided into three sections: temperature range A (900°C–1000°C), B (1000°C–1200°C) and C (1200°C–1300°C).

Temperature range A (900°C–1000°C): In this section, the SSA of the char decreased by 145.46 $m^2/g$, which is much larger than that in section B. The polycondensation of the char generally occurs mainly below 1000°C; therefore the SSA variation of the char might be attributed mainly to the char polycondesation. Besides, Fig. 3(a) and 3(b) indicate that the ash fusion is too slight to be considered. Meanwhile the tiny decrease of the char SSA during the gasification and combustion process proved that the effect of ash sintering is insignificant on the SSA of char.

Temperature range B (1000°C–1200°C): In this section, as the pyrolysis temperature rises, the SSA of the char decreased by merely 57.32 $m^2/g$, which indicates the decline in variation tendency. By the time, the effect of the char polycondensation gradually decreases. The increasing number of the ash droplets in Fig. 3(b), 3(c) and 3(d) demonstrated that the melting ash could block up the pore of char, which greatly leads to the SSA decrease of the char.

Temperature range C (1200°C–1300°C): From the analysis of Fig. 3(f), the molten ash occupies the partial pore of the char or covers the exit of the pore, both of which lead to the SSA decrease of the char.

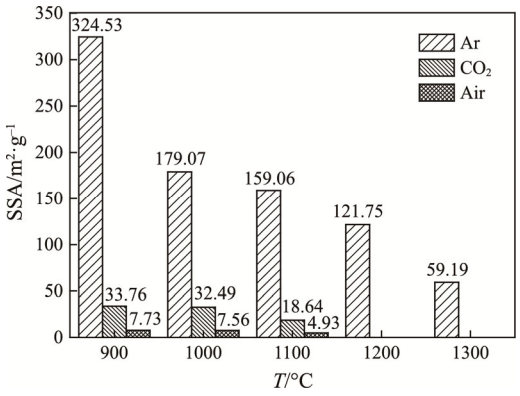


**Fig. 6** SSA of bituminous char/ash prepared at different temperatures

### 3.3 Effect of pyrolysis temperature on the elemental composition of char

During the structure evolution process, the elemental composition is of vital importance which directly concerns the slagging and fouling behaviors. XRF was used to investigate the element composition in char prepared at different pyrolysis temperatures and compared with that of the raw coal. The results are shown in Fig. 7.

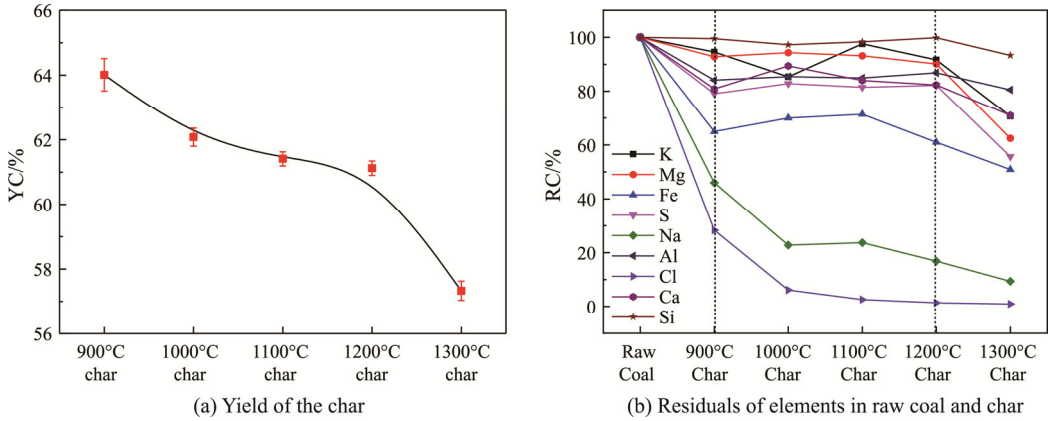


(a) Yield of the char (b) Residuals of elements in raw coal and char

**Fig. 7** Residuals of elements in raw coal and char prepared in different pyrolysis temperatures

The original data of XRF merely gives the relative percentage of the elements in the tested sample. However, it could not directly illustrate the migration changes of the elements from raw coal to char during the heating process. Thus, an index-residual in char (RC) was used to evaluate the residual percentage of elements in char compared with raw coal [55, 56]. The formulas of the RC are as follows.

$$\mathrm{RC} = \mathrm{YC}\frac{\text{elemental content in char}}{\text{elemental content in raw coal}} \tag{1}$$

$$\mathrm{YC} = \frac{m_{\mathrm{char}}}{m_{\mathrm{coal}}} \times 100\% \tag{2}$$

where YC is the yield ratio of char. $m_{\mathrm{char}}$ is the weight of char after pyrolysis, and $m_{\mathrm{coal}}$ is the weight of raw coal used for pyrolysis.

Based on the formulas above mentioned, the yield of char and RC were calculated, and the results are shown in Fig. 7. According to the release in a gaseous state, the elements were divided into three types: (1) Almost non-release, such as Si. Although Si might undergo a series of decomposition or combination process, the RC is nearly invariable from beginning to end. There is no gaseous release of the Si but the occurrence forms of the element have changed. (2) Partly release, for instance, Fe, Al, S, Ca, Mg, K, etc. Among them, the release of K, Mg and Ca mainly occurs across the ash fusion temperature range (900°C–1300°C), while Fe and Al are released before this temperature range (below 900°C). The release of S mainly takes place below 900°C and above 1200°C; the reason could be attributed to the volatilization and decomposition of sulfate, respectively. (3) Almost complete-release, for example, Na, Cl etc. When the coal was pyrolyzed above the ash melting temperature, Na and Cl were respectively reduced by 91% and 99%, which is consistent with the conclusions of Liu et al. [57].

### 3.4 Effect of pyrolysis temperature on the mineral transformation of char

To discuss the composition variation of minerals in depth, and further obtain the mechanism of the interaction between fixed carbon and mineral matter, X-ray diffractions of the char prepared at different pyrolysis temperatures were carried out and compared with those of raw coal. The results are shown in Fig. 8.

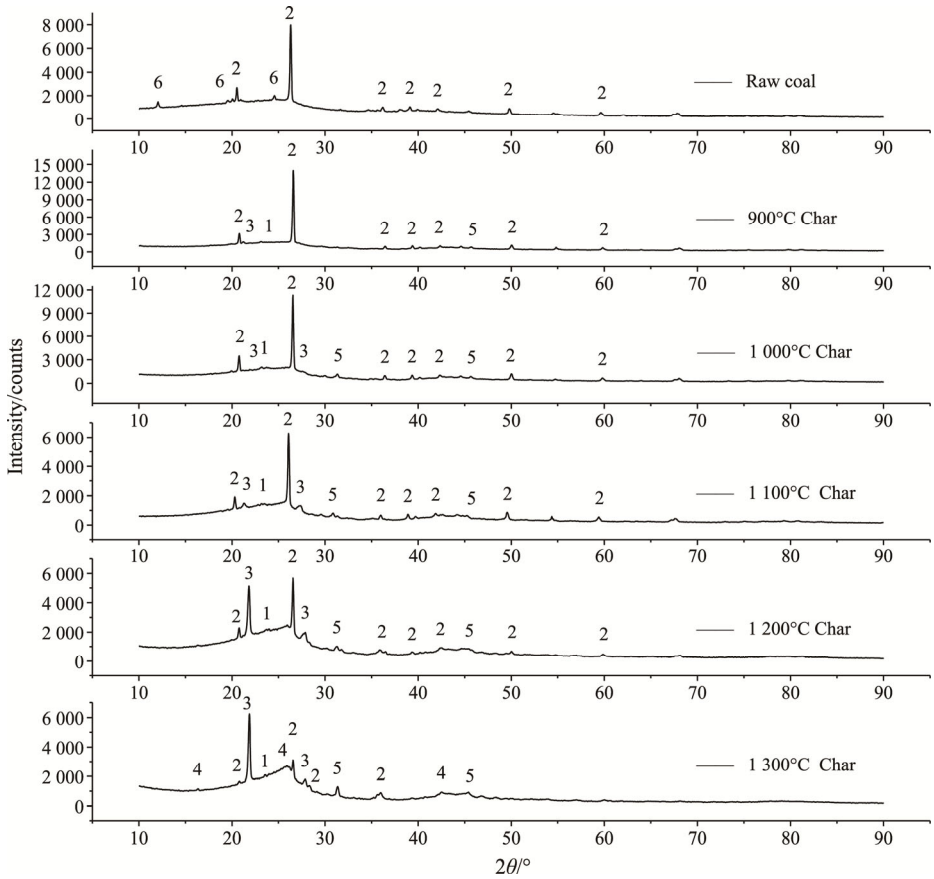


1. Anhydrite; 2. Quartz; 3. Anorthite; 4. Mullite; 5. Oldhamite; 6. Kaolinite

**Fig. 8** XRD patterns of major minerals in raw coal and char prepared at different pyrolysis temperatures

Meanwhile, for some of the reactions during the char structure evolution, FactSage7.3 was used to calculate the Gibbs free energy change ($\Delta G$) of the reaction between minerals at different temperatures.

The XRD results show the major minerals in the raw coal are quartz and clay minerals. The diffraction intensity of kaolinite is the highest in all clay minerals. Nevertheless, none of the diffraction peaks of kaolinite was searched in the XRD patterns of the char. The reactions between minerals may occur as shown in Eqs. (3) and (4); the kaolinite loses crystal water and becomes metakaolinite. With the pyrolysis temperature increasing, the metakaolinite decomposes into mullite and quartz, which is consistent with the XRD patterns.

$$\text{Kaolinite}\left(\left[Al_2O_3\cdot 2SiO_2\cdot 2H_2O\right]\right)\rightarrow \text{Metakaolinite}\left(Al_2O_3\cdot 2SiO_2\right)+2H_2O \tag{3}$$

$$\text{Metakaolinite}\left(Al_2O_3\cdot 2SiO_2\right)\rightarrow \text{Mullite}\left(3Al_2O_3\cdot 2SiO_2\right)+\text{Quartz}\left(SiO_2\right) \tag{4}$$

When the pyrolysis temperature is 900°C, the quartz still exists in the coal char. However, different from raw coal, the diffraction peaks of kaolinite disappeared and some other diffraction peaks emerged such as anhydrite, oldhamite and anorthite. One part of the anhydrite is derived from the minerals of the raw coal, and the other part might be the reaction product of the oxysulfide of coal and calcium oxide, which is generated from the decomposition of the calcite. The relative reactions are listed as Eqs. (5) and (6). As Eq. (6) indicated, the self-decomposition of anhydrite is impossible at 900°C for the thermodynamic limitations. However, the carbon in char could impel the decomposition of the anhydrite, which would cause the generation of oldhamite as Eq. (7). From another perspective, the anhydrite would facilitate the gasification or combustion reaction to some extent. In addition, as Eq. (8), the calcium oxide could also react with the quartz and aluminum oxide, which could reasonably explain the emergence of anorthite in the XRD patterns.

With pyrolysis temperature rising, the diffraction intensities of oldhamite and anorthite in char particles both increase, which demonstrates that both of them have higher stability under the Ar atmosphere in the temperature range 900°C–1300°C. The diffraction intensity of quartz dramatically decreases for the reason of generating anorthite. Especially for 1200°C, consistent with Li et al. [58] and Bai et al. [59], the diffraction intensity of anorthite obviously increases. Bai et al. [59] speculated that partial gehlenite would transform into anorthite for the higher stability at this temperature. In other words, gehlenite is the precursor of anorthite. FactSage7.3 calculation of this reaction as Eq. (9) could verify their speculation to some extent.

Mullite was detected in the XRD patterns of char prepared at 1300°C and the reaction is listed as Eq. (10). Kong at al. [60] also observed the existence of mullite in the slag with residual carbon at 1300°C, while it did not appear at 1200°C. This is consistent with our XRD results. Bai et al. [59] found that when the ash preparing temperature was in the range of 1200°C–1300°C, the content of mullite in Huainan coal ash significantly increases; specifically speaking, the content of mullite in 1300°C was 2.5 times as high as that at 1200°C. The chemical reactions of minerals of bituminous coal char under Ar atmosphere are as follows [50, 59–62]:

$$900°C:\ \text{Calcite}\left(CaCO_3\right)\rightarrow \text{Calcium oxide}\left(CaO\right)+CO_2\left(\Delta G=-0.93\ \text{kJ/mol}\right) \tag{5}$$

$$900°C:\ \text{Anhydrite}\left(CaSO_4\right)\rightarrow \text{Calcium oxide}\left(CaO\right)+SO_3\left(\Delta G=189.63\ \text{kJ/mol}\right) \tag{6}$$

$$900°C:\ \text{Anhydrite}\left(CaSO_4\right)+C\rightarrow \text{Oldhamite}\left(CaS\right)+CO_2\left(\Delta G=-248.93\ \text{kJ/mol}\right) \tag{7}$$

$$900°C:\ CaO+3Al_2O_3+2SiO_2\rightarrow \text{Anorthite}\left(CaO\cdot Al_2O_3\cdot 2SiO_2\right)\left(\Delta G=-129.72\ \text{kJ/mol}\right) \tag{8}$$

$$1200°C:\ \text{Gehlenite}\left(2CaO\cdot Al_2O_3\cdot SiO_2\right)+Al_2O_3+3SiO_2\rightarrow \text{Anorthite}\left(CaO\cdot Al_2O_3\cdot 2SiO_2\right)\left(\Delta G=-101.87\ \text{kJ/mol}\right) \tag{9}$$

$$1300°C:\ 3Al_2O_3+2SiO_2\rightarrow \text{Mullite}\left(Al_6Si_2O_{13}\right)\left(\Delta G=-23.33\ \text{kJ/mol}\right) \tag{10}$$

### 3.5 Effect of pyrolysis temperature on the reactivity of char

A series of char structural evolution, such as micro-morphology, pore structure, elemental composition and mineral transformation of char particles, will affect the reactivity and conversion efficiency of coal char. The research of reactivity could support the structure evolution process of coal char. In order to study the reactivity of char particles prepared by pyrolysis in the ash melting temperature range, the combustion kinetics parameters and characteristic parameters of Lu'an bituminous char were tested through the LabsysEvo thermal analyzer. The ignition temperatures and burnout temperatures were determined by the tangent method

[63]. Kinetic analysis of char combustion was also performed with the widely-used Coats-Redfern method [64, 65]. This method is based on Eq. (11), used as a non-isothermal model.

$$\ln\left[\frac{-\ln(1-\alpha)}{T^2}\right]=\ln\left[\frac{AR}{\beta E}\left(1-\frac{2RT}{E}\right)\right]-\frac{E}{RT} \quad (\text{for } n=1) \quad (11)$$

where, $E$ is the apparent activation energy (kJ/mol); R is the gas constant (8.314 J/K·mol); $\alpha$ is the conversion rate; $A$ is the pre-exponential factor ($min^{-1}$); $\beta$ is the heating rate (K/min); $T$ is the absolute temperature (K). By assuming $2RT \ll E$, in the plot of $\ln(-\ln(1-\alpha)/T^2)$ versus $1/T$, $E$ and $A$ can be obtained from the slope and intercept respectively. The calculation method of combustion stability index-$D_w$, flammability index-$C$ and complex combustion index-$S$ were listed as Eqs. (12)–(14).

$$D_w=\frac{DTG_{max}}{T_i\times T_b} \quad (12)$$

$$C=\frac{DTG_{max}}{T_i^2} \quad (13)$$

$$S=\frac{DTG_{max}\times DTG_{mean}}{T_i^2\times T_b} \quad (14)$$

where $T_i$ is the ignition temperature, and the $T_b$ is the burnout temperature. $DTG_{max}$ is the maximum combustion rate obtained from the DTG curve. $DTG_{mean}$ is the average combustion rate calculated from the DTG curve. The results of combustion kinetics parameters and characteristic parameters are shown in Tables 3 and 4. Table 3 gives the kinetics parameters of coal char in the combustion process. The higher the pyrolysis temperature, the higher the activation energy of the char combustion reaction. Furthermore, the pre-exponential factor of coal char rises with the pyrolysis temperature, indicating that the number of activated molecules corresponding to the activation energy also increases. In addition, we also found that there is a dynamic compensation effect between the apparent activation energy and pre-exponential factors of the combustion kinetic parameters of bituminous coal char prepared at different temperatures, as shown in Fig. 9. The validity of the compensation effect is not generally accepted and it is often considered as a statistical deviation, while previous researchers [66–68] proved the importance of the compensation effect on the kinetic parameters and gave several theoretic interpretations for that phenomenon. From Table 4, it could be seen that with the increase of pyrolysis temperature, both ignition and burnout temperatures of char samples increase. The ignition and burnout of the char should be delayed correspondingly. In addition, all the combustion indexes of coal char decrease with the increase of pyrolysis temperature, which indicates that the increase of pyrolysis temperature leads to the combustion stability decrease of coal char.

**Table 3** Effect of pyrolysis temperature on kinetics parameters of coal char in combustion process

| Pyrolysis temperature/°C | Activation energy/kJ·mol$^{-1}$ | Pre-exponential factors/min$^{-1}$ | $R^2$ |
|---|---|---|---|
| 900 | 89.26 | 29 879.4 | 0.992 31 |
| 1000 | 100.73 | 91 524.1 | 0.995 29 |
| 1100 | 108.96 | 175 787.8 | 0.995 35 |
| 1200 | 124.46 | 829 440.9 | 0.995 28 |
| 1300 | 131.91 | 1 668 007.0 | 0.994 59 |

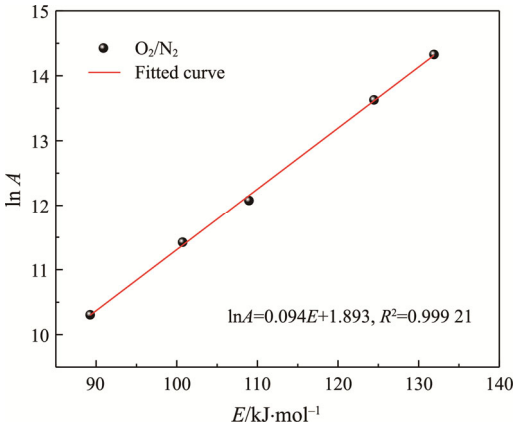


**Fig. 9** Dynamic compensation effect analysis curve under $O_2/N_2$ atmosphere

**Table 4** Effect of pyrolysis temperature on characteristic parameters of coal char in combustion process

| Pyrolysis temperature /°C | Ignition temperature /°C | Burnout temperature /°C | Combustion stability index /%·min$^{-1}$·K$^{-2}$ | Flammability index /%·min$^{-1}$·K$^{-2}$ | Complex combustion index /%$^2$·min$^{-2}$·K$^{-3}$ |
|---|---|---|---|---|---|
| 900 | 492.92 | 668.68 | 1.156 02E–05 | 1.568 23E–05 | 1.456 83E–08 |
| 1000 | 506.98 | 706.72 | 1.102 64E–05 | 1.537 05E–05 | 1.432 20E–08 |
| 1100 | 542.51 | 738.34 | 1.031 45E–05 | 1.403 77E–05 | 1.219 42E–08 |
| 1200 | 574.12 | 767.99 | 9.557 48E–06 | 1.278 49E–05 | 1.076 01E–08 |
| 1300 | 601.82 | 785.61 | 9.548 98E–06 | 1.246 52E–05 | 9.970 09E–09 |

## 4. Conclusions

An experimental study on Lu'an bituminous coal char/ash structure evolution at around ash melting temperature was performed under three atmospheres ($Ar/CO_2$/air) on a laboratory-scale fixed bed. The SEM-EDS, SSA, XRF, XRD and TGA were carried out to obtain the variation of the morphology, specific surface area, element composition, mineral transformation and char combustion reactivity with the increasing temperature, respectively. The conclusions are as follows:

(1) During the rise in pyrolysis temperature from 900°C to 1300°C, the number density and geometry size of the ash spheres on char particle surface increase significantly, and the phenomenon of ash spheres coalescence more pronounced. Exudation, agglomeration and coalescence of molten ash may block the pores in char structure and cause the SSA loss of char. The large ash particles and ash fragments can both be observed under gasification in $CO_2$ and combustion in air. Ash fragments increase with the reaction temperature, which demonstrates that all the minerals in char are not fully connected to form an ash skeleton.

(2) The residual content of chloride in the char becomes 1% and the contents of Fe, K, Mg and Na decrease significantly during the pyrolysis temperature across the ash melting temperature zone. The existence of oldhamite gives an evidence of the interaction between carbon and minerals; carbon could impel decomposition of the anhydrite to generate oldhamite. With pyrolysis temperature rising, the diffraction intensity of oldhamite and anorthite both increase because their high stability and the diffraction intensity of quartz dramatically decrease due to anorthite generation.

(3) With the increase of pyrolysis temperature, both ignition and burnout temperatures of char increase and the combustion stability of the char decreases. The higher the pyrolysis temperature, the higher the activation energy of char combustion reaction. There is a dynamic compensation effect between the apparent activation energy and pre-exponential factors of the combustion kinetic parameters of bituminous coal char prepared at different temperatures.

## Acknowledgments

The financial support from the Natural Science Fund of China (51576158) is gratefully acknowledged. We also thank the support of the Instrument Analysis Center of Xi'an Jiaotong University.

## References

[1] Lv P., Bai Y.H., Yang X.H., et al., Impacts of char structure evolution and inherent alkali and alkaline earth metallic species catalysis on reactivity during the coal char gasification with $CO_2/H_2O$. International Journal of Energy Research, 2018, 42 (11): 3633–3642.

[2] Lourival J., Mendes N., Edson Bazzo J., Toste Azevedo, Thermal conductivity analysis of an ash deposit on boiler superheater. Powder Technology, 2017, 318, 329–336.

[3] Zhang Y.K., Zhang H.X., Zhu Z.P., et al., Physicochemical properties and gasification reactivity of the ultrafine semi-char derived from a bench-scale fluidized bed gasifier. Journal of Thermal Science, 2017, 26(4): 362–370.

[4] Lu J.T., Huang J.Y., Yang Z., et al., Effect of cobalt content on the oxidation and corrosion behavior of ni–fe-based superalloy for ultra-supercritical boiler applications. Oxidation of Metals, 2017, 89(1–2): 197–209.

[5] Kleinhans U., Wieland C., Frandsen F.J., et al., Ash formation and deposition in coal and biomass fired combustion systems: Progress and challenges in the field of ash particle sticking and rebound behavior. Progress in Energy and Combustion Science, 2018, 68: 65–168.

[6] Helble J.J., DeVito M.S., Wu C.Y., et al., Combustion aerosols: factors governing their size and composition and implications to human health. Journal of the Air & Waste Management Association, 2000, 50(9): 1619–1622.

[7] Benson S.A., Sondreal E.A., Hurley J.P., Status of coal ash behavior research. Fuel Processing Technology, 1995, 44: 1–12.

[8] Yang W.J., Zhao J.H., Cao X.Y., et al., Research on the slagging characteristics of Shenhua coal. Asia-Pacific Journal of Chemical Engineering, 2007, 2: 171–176.

[9] Wang Q., Han K.H., Qi J.H., et al., Investigation of potassium transformation characteristics and the influence of additives during biochar briquette combustion. Fuel, 2018, 222: 407–415.

[10] Montagnaro F., Brachi P., Salatino P., Char-wall interaction and properties of slag waste in entrained-flow gasification of coal. Energy & Fuels, 2011, 25: 3671–3677.

[11] Zhu Z.B., M. Z.H., Lin S.Y., et al., Characteristics of coal char gasification at high temperature: (Ⅰ) The effect of ash fusion on coal char gasification. CIESC Journal, 1994, 2: 147–154.

[12] Liu Y.H., Xu S.J., Zhang Y.J., et al., Lignite gasification characteristics in a cyclone slagging gasifier. Journal of Combustion Science and Technology, 2018, 24: 120–125.

[13] Dai B.Q., Wu X.J., Zhao J., et al., Xinjiang lignite ash slagging and flow under the weak reducing environment at high temperatures-slag viscosity and its variation with ash type and addition of clay. Fuel, 2019, 245: 438–446.

[14] Feng B., Bhatia S.K., Variation of the pore structure of coal chars during gasification. Carbon, 2003, 41(3): 507–523.

[15] Shen C.M., Lin W.G., Wu S.H., et al., Experimental study of combustion characteristics of bituminous char derived under mild pyrolysis conditions. Energy & Fuels, 2009, 23(11): 5322–5330.

[16] Liu J.X., Jiang X.M., Shen J., et al., Influences of particle size, ultraviolet irradiation and pyrolysis temperature on stable free radicals in coal. Powder Technology, 2015, 272: 64–74.

[17] Casal M.D., Vega M.F., Diaz-Faes E., et al., The influence of chemical structure on the kinetics of coal pyrolysis. International Journal of Coal Geology, 2018, 195: 415–422.

[18] Bai Y.H., Lv P., Yang X.H., et al., Gasification of coal char in $H_2O/CO_2$ atmospheres: Evolution of surface morphology and pore structure. Fuel, 2018, 218: 236–246.

[19] Fuentescano D., Parrillo F., Ruoppolo G., et al., The influence of the char internal structure and composition on heterogeneous conversion of naphthalene. Fuel Processing Technology, 2018, 172: 125–132.

[20] Xie K.C., Coal structure and its reactivity, Peking: Science Press, 2002.

[21] Senneca O., Bareschino P., Urciuolo M., et al., Prediction of structure evolution and fragmentation phenomena during combustion of coal: Effects of heating rate. Fuel Processing Technology, 2017, 166: 228–236.

[22] Bai J., Li W., Li C.Z., et al., Influences of minerals transformation on the reactivity of high temperature char gasification. Fuel Processing Technology, 2010, 91(4): 404–409.

[23] Mukherjee S., Srivastava S.K., Minerals transformations in northeastern region coals of india onheat treatment. Energy & Fuels, 2006, 20: 1089–1096.

[24] Ma Z.B., Bai J., Bai Z.Q., et al., Mineral transformation in char and its effect on coal char gasification reactivity at high temperatures, part 2: char gasification. Energy & Fuels, 2014, 28(3): 1846–1853.

[25] Wu X.J., Zhang Z.X., Piao G.L., et al., Behavior of mineral matters in chinese coal ash melting during char-$CO_2/H_2O$ gasification reaction. Energy & Fuels, 2009, 23: 2420–2428.

[26] Wang S., Wu L.P., Hu X., et al., An X-ray photoelectron spectroscopic perspective for the evolution of O-containing structures in char during gasification. Fuel Processing Technology, 2018, 172: 209–215.

[27] Ma Z.B., Bai J., Li W., et al., Mineral transformation in char and its effect on coal char gasification reactivity at high temperatures, part 1: mineral transformation in char. Energy & Fuels, 2013, 27(8): 4545–4554.

[28] Radovic L., Importance of catalyst dispersion in the gasification of lignite chars. Journal of Catalysis, 1983, 82(2): 382–394.

[29] Ding L., Zhou Z.J., Guo Q.H., et al., In-situ analysis and mechanism study of char-ash/slag transition in pulverized coal gasification. Energy & Fuels, 2015, 29(6): 3532–3544.

[30] Luan J.Y., Wu X.M., Wu G.F., et al., Analysis of char specific surface area and porosity from the fast pyrolysis of biomass and pulverized coal. Advanced Materials Research, 2013, 608–609: 383–387.

[31] Wang M.M., Zhang J.S., Zhang S.Y., et al., Effect of pyrolysis conditions on the structure and gasification reactivity of char. Coal Conversion, 2007, 3: 21–24.

[32] Zhang S.Y., Lu J.F., Zhang J.S., et al., Effect of pyrolysis intensity on the reactivity of coal char. Energy & Fuels, 2008, 22(5): 3213–3221.

[33] Wei J.T., Guo Q.H., Ding L., et al., Understanding the effect of different biomass ash additions on pyrolysis product distribution, char physicochemical characteristics, and char gasification reactivity of bituminous coal. Energy & Fuels, 2019, 33(4): 3068–3076.

[34] Raask E., Slag-coal interface phenomena. Journal of Engineering for Power, 1966, 88(1): 40–44.

[35] Lin S.Y., Hirato M., Horio M., The characteristics of coal char gasification at around ash melting temperature. Energy & Fuels, 1994, 8(3): 598–606.

[36] Miccio F., Salatino P., Tina W., Modeling gasification and percolation of ash-bearing porous carbon particles. Proceedings of the Combustion Institute, 2000, 28(2): 2163–2170.

[37] Latorre A.C.D., Ash formation under pressurized pulverized coal combustion conditions. University of Connecticut, 2005.

[38] Wu S.Y., Zhang X., Gu J., et al., Interactions between carbon and metal oxides and their effects on the carbon/$CO_2$ reactivity at high temperatures. Energy & Fuels, 2007, 21(4): 1827–1831.

[39] Wang J., Morishita K., Takarada T., High-temperature interactions between coal char and mixtures of calcium oxide, quartz, and kaolinite. Energy & Fuels, 2001, 15(5): 1145–1152.

[40] Wang J., Kong L.X., Bai J., et al., The role of residual char on ash flow behavior, Part 2: Effect of $SiO_2/Al_2O_3$ on ash fusibility and carbothermal reaction. Fuel, 2019, 255: 1146–1158.

[41] Nowok J.W., Hurley J.P., Benson S.A., The role of physical factors in mass transport during sintering of coal ashes and deposit deformation near the temperature of glass transformation. Fuel Processing Technology, 1998, 56(1–2): 89–101.

[42] Jung B., Sintering characteristics of low-rank coal ashes.

Korean Journal of Chemical Engineering, 1996, 13(6): 633–639.

[43] Gray V.R., Prediction of ash fusion temperature from ash composition for some New Zealand coals. Fuel, 1987, 66(9): 1230–1239.

[44] Liu M., Shen Z.J., Liang Q.F., et al., New slag-char interaction mode in the later stage of high ash content coal char gasification. Energy & Fuels, 2018, 32(11): 11335–11343.

[45] Zhang Y.D., Liu Y.H., Duan X.L., et al., Effect of temperature on Lu'an bituminous char structure evolution in pyrolysis and combustion. Frontiers in Energy, 2021, 15: 14–25.

[46] Vassilev S.V., Tascon J.M.D., Methods for characterization of inorganic and mineral matter in coal: A critical overview. Energy Fuels, 2003, 17: 271–228.

[47] Gupta R., Advanced coal characterization: A review. Energy Fuels, 2007, 21: 451–460.

[48] Markus R., Marcus S., Stefan G., et al., Ash behavior of various fuels: The role of the intrinsic distribution of ash species. Fuel, 2019, 253: 930–940.

[49] Bale C.W., Degterov S.A., Eriksson G., et al., FactSage thermochemical software and databases, 2010–2016. Calphad, 2016, 54: 35–53.

[50] Ma Z.B., Bai J., Wen X.D., et al., Mineral transformation in char and its effect on coal char gasification reactivity at high temperatures, part 3: Carbon thermal reaction. Energy & Fuels, 2014, 28: 3066–3073.

[51] Zhang H., Li X.Y., Scanning electron microscope in the application of coal petrography. Journal of Chinese Electron Microscopy Society, 2004, 23(4): 467–467.

[52] Wang Q., Han K.H., Wang J.M., et al., Influence of phosphorous based additives on ash melting characteristics during combustion of biomass briquette fuel. Renewable Energy, 2017, 113: 428–437.

[53] Hüttinger K.J., Transport and other effects in coal gasification. In: Yürüm Y. (eds), New Trends in Coal Science. NATO ASI Series, vol. 244. Springer, Dordrecht, 1988. DOI: 10.1007/978-94-009-3045-2_21.

[54] Shen Z.J., Zhang L.Q., Liang Q.F., et al., In situ experimental and modeling study on coal char combustion for coarse particle with effect of gasification in air ($O_2/N_2$) and $O_2/CO_2$ atmospheres. Fuel, 2018, 233: 177–187.

[55] Lorenz H., Carrea E., Tamura M., et al., The role of char surface structure development in pulverized fuel combustion. Fuel, 2000, 79(10): 1161–1172.

[56] Matzakos A., Zygourakis K., Pyrolysis of plastic coals: Pore structure development and char reactivity. 1990, 35: 2.

[57] Liu S.Q., Tang X.N., Zhang B., et al., Characterization of halogen elements emissions from coal gasification and combustion by equilibrium calculation. Computer and Applied Chemistry, 2016, 28: 1165–1171.

[58] Li W., Chemistry of coal ash, Peking, Science Press, 2013.

[59] Bai J., Li W., Bai Z.Q., et al., Transformation of mineral matters in yanzhou coal ash at high temperature. Journal of China University of Mining and Technology, 2008, 37(3): 369–372.

[60] Kong L.X., Jin B., Li W., et al., The internal and external factor on coal ash slag viscosity at high temperatures, Part 2: Effect of residual carbon on slag viscosity. Fuel, 2015, 158: 976–982.

[61] Li H.F., Huang J.J., Fang Y.T., et al., Formation mechanism of slag during fluid-bed gasification of lignite. Energy & Fuels, 2011, 25: 273–280.

[62] Liu Z., Li J.B., Zhu M.M., et al., Morphological and mineralogical characterisation of ash deposits during circulating fluidized bed combustion of zhundong lignite. Energy & Fuels, 2019, 33: 2122–2132.

[63] Ma B.G., Li X.G., Xu L., et al., Investigation on catalyzed combustion of high ash coal by thermogravimetric analysis. Thermochimica Acta, 2006, 445: 19–22.

[64] Coats A.W., Redfern J.P., Kinetic parameters from thermogravimetric data. Nature, 1964, 201 (4914): 68–69.

[65] Hu W.H., Liang F., Xiang H.Z., et al., Investigating co-firing characteristics of coal and masson pine. Renewable Energy, 2018, 126: 563–572.

[66] George S., Catalysis and compensation effect of $K_2CO_3$ in low-rank coal – $CO_2$ gasification. Central European Journal of Chemistry, 2013, 11(7): 1187–1200.

[67] Galwey A.K., Compensation effect in heterogeneous catalysis. Advances in Catalysis, 1977, 26(2): 247–322.

[68] Bond, Geoffrey C., The significance of the compensation effect and the definition of active centres in metal catalysts. Ztschrift Für Physikalische Chemie, 1985, 144: 21–31.